# Sharp kinetic acceleration potentials during mediated redox catalysis of insulators

**Deqing Cao**
Nanjing Tech University
**Xiaoxiao Shen**
Nanjing Tech University
**Aiping Wang**
Shanghai University
**Fengjiao Yu**
Nanjing Tech University
**Yuping Wu**
Nanjing Tech University
**Siqi Shi**
Shanghai University
**Stefan Freunberger** ( stefan.freunberger@ist.ac.at )
Institute of Science and Technology Austria https://orcid.org/0000-0003-2902-5319
**Yuhui Chen**
Nanjing Tech University

**Article**

**Keywords:**

**DOI:** https://doi.org/10.21203/rs.3.rs-750965/v1

# Sharp kinetic acceleration potentials during mediated redox catalysis of insulators

Deqing Cao[1+], Xiaoxiao Shen[1+], Aiping Wang[2], Fengjiao Yu[1], Yuping Wu[1], Siqi Shi[2,4]*, Stefan A. Freunberger[3]*, Yuhui Chen[1]*

[1] State Key Laboratory of Materials-oriented Chemical Engineering, College of Chemical Engineering, Nanjing Tech University, Nanjing, Jiangsu, 211816 China

[2] School of Materials Science and Engineering, Shanghai University, Shanghai 200444, China

[3] IST Austria (Institute of Science and Technology Austria), Klosterneuburg, Austria

[4] Materials Genome Institute, Shanghai University, Shanghai 200444, China

Corresponding authors: cheny@njtech.edu.cn; sqshi@shu.edu.cn; stefan.freunberger@ist.ac.at

[+] Authors contributed equally to this work.

**Redox mediators could catalyse otherwise slow and energy-inefficient cycling of Li-S and Li-$O_2$ batteries by shuttling electrons/holes between the electrode and the solid insulating storage materials. For mediators to work efficiently they need to oxidize the solid with fast kinetics yet the lowest possible overpotential. Here, we found that when the redox potentials of mediators are tuned via, e.g., $Li^+$ concentration in the electrolyte, they exhibit distinct threshold potentials, where the kinetics accelerate several-fold within a range as small as 10 mV. This phenomenon is independent of types of mediators and electrolyte. The acceleration originates from the overpotentials required to activate fast $Li^+/e^-$ extraction and the following chemical step at specific abundant surface facets. Efficient redox catalysis at insulating solids requires therefore carefully considering the surface conditions of the storage materials and electrolyte-dependent redox potentials, which may be tuned by salt concentrations or solvents.**

Electrochemistry with insulators is salient feature and central difficulty of topical future battery chemistries such as Li-air ($O_2$), Li-$CO_2$, Li-Sulphur (Li-S) cells[1-10]. They differ in this respect from current intercalation-type batteries, which rely on ion (de)insertion to balance charge upon redox of the mixed-conducting solid host[1]. The interest in Li-$O_2$, -$CO_2$, and -S cells arises from high theoretical energies, abundant elements, low cost and environmental friendliness. Li-$O_2$/$CO_2$ cells interconvert $O_2$ dissolved in the electrolyte into solid, insulating $Li_2O_2$ or $Li_2CO_3$ during discharge/charge. Li-S batteries interconvert solid, insulating $S_8$ and $Li_2S$. Kinetic bottleneck during these processes is charge transfer between electrode and the insulating, insoluble, solid storage materials, causing high overpotentials and incomplete conversion even at low rates.

Redox catalysis using mediators can bypass those insulators, transporting charge through the electrolyte phase where ion and electron/hole transport may be facile and may boost charge transfer kinetics[3-5,11-14]. Equally important is to approach the cycling potential as close as possible towards the formal potential of the storage material to maximize energy efficiency and to suppress parasitic reactions[4,5,15-21]. Soluble redox mediators (RMs) are, therefore, now accepted to be key to achieve these goals and have been studied in a wide variety for Li-$O_2$ cells[3-5,11-13,18,21-24]. First examples have been reported for S electrochemistry[3,25-27]. Redox mediation on, for example, charging involves oxidizing the mediator $RM^{red}$ at the electrode surface to its oxidized form $RM^{ox}$, its diffusion to the surface of $Li_2O_2$ or $Li_2S$, where $RM^{ox}$ extracts charge and reforms $RM^{red}$. Main requirements for successful redox catalysis include a suitable equilibrium potential of the redox couple to drive the reaction and fast heterogeneous reaction rates between RM and both electrode ($k^0$) and storage material. $k^0$ is sufficiently fast[28] and well described by established theories of electron transfer between redox molecule and metallic conductor[29]. However, for the rate limiting electron transfer between $RM^{ox}$ and a redox active insulating solid, despite being essential, detailed descriptors are missing.

Activating this most difficult electron transfer step is the primary goal of redox catalysis on charging Li-S and Li-$O_2$ batteries, which have important parallels in their charging reactions. The insulating $Li_2S$ and $Li_2O_2$ undergo in a first step a one-electron oxidation to form Li polysulfides (LiPSs) or Li superoxide ($LiO_2$) intermediates. Further oxidation and/or disproportionation eventually yields the most oxidized forms $S_8$ and $O_2$, respectively[10,20,30-32]. Reaction kinetics for $RM^{ox}$ and $Li_2O_2$ were reported for a range of mediators, typically assuming faster kinetics with higher mediator potential (driving force)[28,33,34]. Impacts of solvents have been noted on the redox potentials of mediators and the $Li/Li^+$ redox couple[15,35]. For mediated $Li_2S$ oxidation, faster mediated compared to unmediated kinetics were phenomenologically inferred from potentiostatic titration or galvanostatic cycling[25-27]. However, quantitative relations between electrolyte-dependent redox potentials of mediators and the kinetics of mediated oxidation of insulating solids are missing, yet this knowledge is essential for mediated redox catalysis of insulators.

Here, we investigate the kinetics of mediated $Li_2S$ and $Li_2O_2$ oxidation upon varying the redox potential of particular mediators by means of $Li^+$ concentration and electrolyte solvent. We find that the kinetics show distinct threshold potentials, where the kinetics accelerates several-fold within a voltage range of as little as 10 mV. We show that the thresholds originate from the

overpotentials to activate fast $Li^+/e^-$ extraction followed chemical steps. Overpotentials are different amongst facets and, therefore, thresholds indicate abundant facets.

## Results

### Thresholds in the potential-dependent kinetics of RMs oxidizing $Li_2S$ and $Li_2O_2$

Decamethyl ferrocene (DFc) and lithium iodide (LiI) are commonly used RMs for the charging process in Li-S batteries and Li-$O_2$ batteries, respectively, and thus they are chosen as model RMs in this work[14]. Their redox potentials, $E_{\mathrm{DFc/DFc^+}}$ and $E_{\mathrm{I^-/I_3^-}}$, measured on the AgCl/Ag scale are nearly independent of $Li^+$ concentration because of the species' large radii and weak solvation, while $E_{\mathrm{Li/Li^+}}$ does vary with $Li^+$ concentration following Nernst equation. Hence, $E_{\mathrm{DFc/DFc^+}}$ and $E_{\mathrm{I^-/I_3^-}}$ vs Li/$Li^+$ vary with $Li^+$ concentration as shown in Supplementary Fig. 1.

Figure 1 shows the potential-dependent apparent rate constants $k^{\mathrm{app}}$ of $DFc^+$ and $I_3^-$ oxidizing $Li_2S$ and $Li_2O_2$, respectively. The rate constant for $DFc^+$ oxidizing $Li_2S$ ($k^{\mathrm{app}}_{\mathrm{DFc-Li_2S}}$) was measured by following the $DFc^+$ concentration of a solution in contact with $Li_2S$ using UV-Vis spectroscopy (see Methods and Supplementary Figure S2). The rate constant of $I_3^-$ oxidizing $Li_2O_2$ ($k^{\mathrm{app}}_{\mathrm{I_3^- - Li_2O_2}}$) was measured using both scanning electrochemical microscopy (SECM) and differential electrochemical mass spectrometry (DEMS) as detailed in Supplementary Note 1. Given the complex mechanism with initial oxidation of $Li_2S$ or $Li_2O$ followed by further oxidation of the intermediates or their disproportionation, apparent rate constants embrace all $e^-$ transfer steps. In either case, the rates followed first-order behaviour in $RM^{ox}$ concentration. They increase with increasing mediator equilibrium potential. Surprisingly, however, is that in both cases kinetics increased sharply by a factor of ~3 to 4.4 over a certain narrow range of equilibrium potentials, whereas changes were gradual below and above these potentials. They represents a threshold, where rather slow kinetics at lower potentials switches to much higher levels.

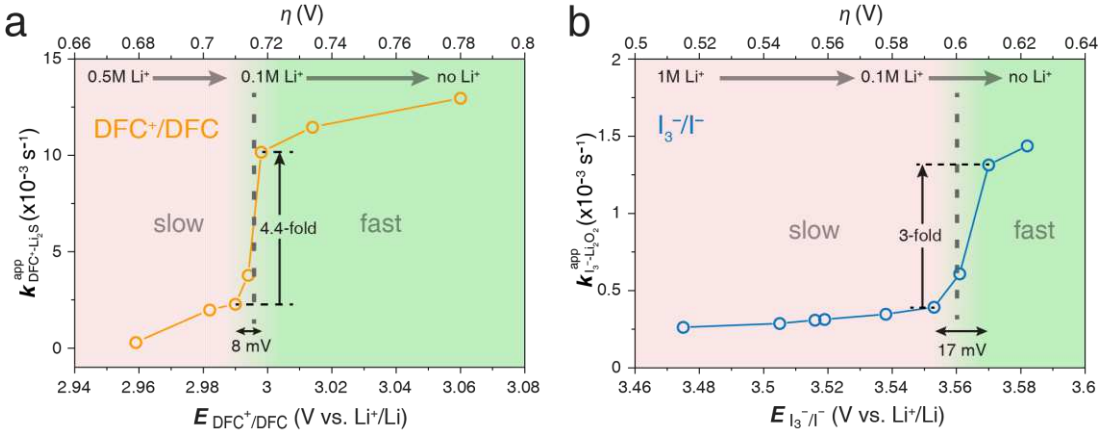


**Fig. 1 | Potential-dependent kinetics of mediated oxidation of $Li_2S$ and $Li_2O_2$. a**, **b**, The apparent reaction rate constants ($k^{\mathrm{app}}$) of as a function of the equilibrium potentials of the mediators. **a**, $k^{\mathrm{app}}_{\mathrm{DFc-Li_2S}}$ of decamethyl ferrocene ($DFc^+$) oxidizing $Li_2S$ with the equilibrium potentials ($E_{\mathrm{DFc/DFc^+}}$) tuned by the $Li^+$ concentration as indicated. The electrolyte was DME containing LiTFSI. The ordinate on the top indicates the overpotential relative to $Li_2S/Li_2S_2$. **b**, Equivalent data for $I_3^-$ oxidizing $Li_2O_2$ ($k^{\mathrm{app}}_{\mathrm{I_3^- - Li_2O_2}}$) with various $E_{\mathrm{I^-/I_3^-}}$ in DMSO electrolyte containing LiTFSI. Thresholds were identified at 2.995 V and 3.56 V vs. $Li^+$/Li, respectively.

For $DFc^+$ oxidizing $Li_2S$, this distinct threshold was at ~2.995 V vs. $Li/Li^+$ in 1,2-dimethoxyethane (DME), Fig. 1a. When the $Li^+$ concentration decreased from 0.15 M to 0.1 M, $E_{DFc/DFc^+}$ only slightly increased by 8 mV to 2.998 V, while $k^{app}_{DFc-Li_2S}$ was boosted 4.4-fold from 0.0023 to 0.0102 $s^{-1}$. This threshold corresponds to an overpotential of ~0.72 V versus the equilibrium potential of the $Li_2S/Li_2S_2$ redox couple, the relevant reaction for the first electron transfer step. As a multi-step reaction, the reaction mechanism of $Li_2S$ oxidation is complicated and forms as a first step partly soluble $Li_2S_2$ species as intermediate, which then over a series of oxidation/disproportionation steps eventually forms $S_8$. Therefore, the apparent kinetics could be dominated by the oxidation of either solid $Li_2S$ or soluble polysulfides. To identify the rate-determining step, $DFc^+$ solutions in DME were separately added to two cuvettes with solid $Li_2S$ and Li polysulfide dissolved in DME. The UV-vis spectra of both solutions were recorded after reacting for 150 s. As shown in Supplementary Fig. 3, $DFc^+$ was completely consumed in the reaction with polysulphides, but only partly with $Li_2S$, which indicates that the reaction of $DFc^+$ oxidizing solid $Li_2S$ is slower than oxidizing polysulfides and thus the former is the rate-determining step. Therefore, the threshold of $E_{DFc/DFc^+}$ at 2.995 V in Fig. 1a is associated with the reaction of $DFc^+$ oxidizing solid $Li_2S$ instead of oxidizing soluble polysulfides.

Turning to $I_3^-$ oxidizing $Li_2O_2$, a similar threshold was found around 3.56 V vs. $Li^+/Li$ (between 0.05 and 0.01 M $Li^+$), where the kinetics is accelerated 3-fold over only 17 mV. Our previous work has shown that, again, the first electron extraction to form a superoxide is the rate determining step[20] and, therefore, the threshold of ~3.56 V in Fig. 1b is associated with $I_3^-$ oxidizing solid $Li_2O_2$.

**Factors governing the thresholds**

These astonishing but unambiguous thresholds of $E_{RM^{red}/RM^{ox}}$ at 2.995 V for $Li_2S$ and 3.56 V for $Li_2O_2$ could originate from many factors such as electrolytes, type of RM, or surface properties of $Li_2S$ and $Li_2O_2$. We focus further on $Li_2O_2$ oxidation. Given that $Li^+$ is not involved in the $I_3^-/I^-$ redox couple, $E_{I^-/I_3^-}$ relies on the $Li^+$ activity ($a_{Li^+}$) in the electrolyte as detailed in Supplementary Note 2. It can be manipulated either by directly changing the $Li^+$ concentration in a given solvent or by changing the solvation ability of the electrolyte[35], which changes the activity coefficient ($\gamma$) and $a_{Li^+}$. To prove this, a dimethyl sulfoxide (DMSO)/DME mixture electrolyte with various ratios of DMSO/DME and constant 10 mM $Li^+$ was used to change the solvation of $Li^+$ and thus to manipulate $E_{I^-/I_3^-}$ (Supplementary Fig. 4). Figure 2a compares the resulting apparent kinetics versus $E_{I^-/I_3^-}$ with those obtained with varying $Li^+$ concentrations in pure DMSO. Although tuned differently, an analogous step-change in kinetics at 3.56 V resulted. For example, 10 mM $Li^+$ in DMSO yielded a potential beyond the threshold and fast kinetics while increasing DME raised $Li^+$ activity and lowered the potential below the threshold. As the extreme, $I_3^-$ in contact with $Li_2O_2$ in pure DME evolved almost no $O_2$, Supplementary Fig. 5. Changing kinetics is, hence, not simply arising from the solvent or $Li^+$ concentration, but rather from $a_{Li^+}$ and in turn the potential on the $Li/Li^+$ scale. We conclude that the thresholds is genuinely linked to $E_{I^-/I_3^-}$.

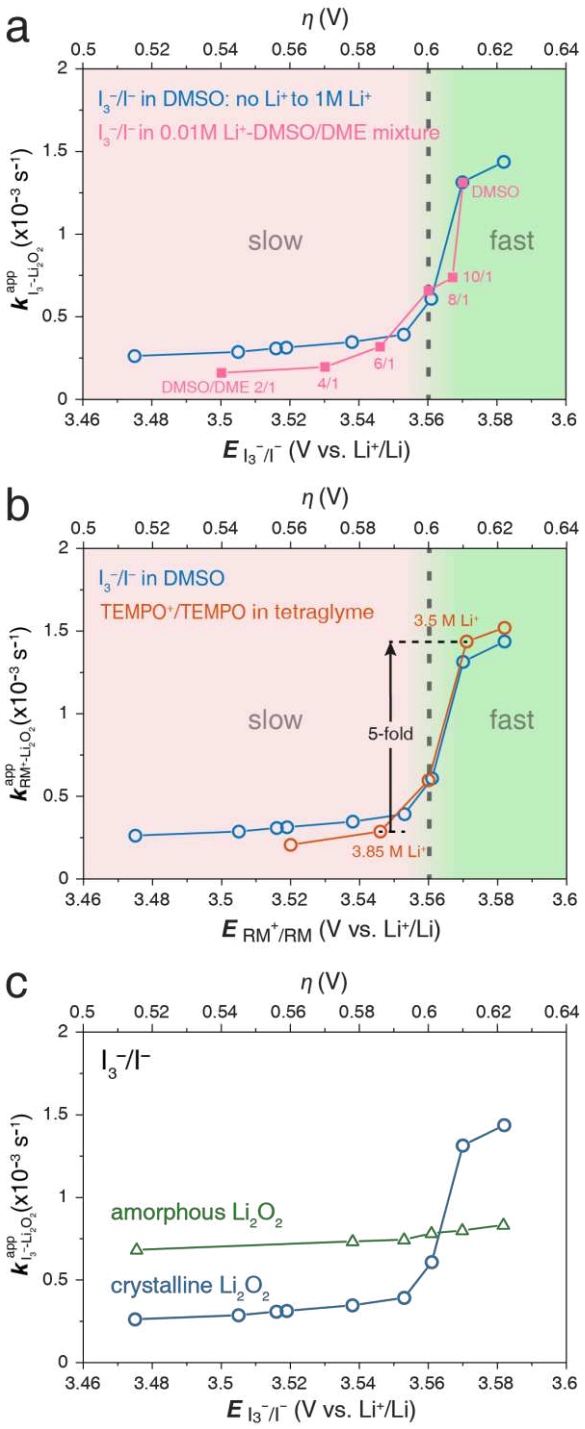


**Figure 2** | **Potential-dependent kinetics of $Li_2O_2$ oxidation in various systems. a,** $I_3^-/I^-$ in DMSO and DMSO/DME mixtures with various ratios; **b,** $TEMPO^+$/TEMPO in tetraglyme electrolytes with various $Li^+$ concentrations. The dashed lines indicate the threshold potentials. **c**, rate constants $k^{app}_{I_3^- - Li_2O_2}$ for oxidizing crystalline $Li_2O_2$ (blue) and amorphous $Li_2O_2$ (green) in DMSO solution with various $Li^+$ concentrations.

To further prove the threshold to be linked to redox potential rather than the particular RM, the same experiments were carried out with 2,2,6,6-tetramethyl-1-piperidinyloxy (TEMPO) and tetraethylene glycol dimethyl ether (tetraglyme) to substitute for LiI and DMSO. Both TEMPO and tetraglyme have been extensively employed in the Li-$O_2$ batteries[18,19]. $O_2$ evolving from $TEMPO^+$ in

contact with $Li_2O_2$ is shown in Supplementary Fig. 6 and the apparent kinetics in Fig. 2b, again compared to the $I_3^-$/DMSO data. From 3.25 M to 4 M $Li^+$, $E_{\mathrm{TEMPO/TEMPO^+}}$ varied from 3.58 V to 3.52 V, covering the previously determined threshold. Again, a similar step-change increasing kinetics 5-fold appeared at ~3.56 V. This result verifies the threshold to be independent of the type of RM or solvent. We show in Supplementary Note 3 that thresholds do not stem from impurities. Together with a similar threshold for $Li_2S$ oxidation at a different overpotential, we conclude that the thresholds are linked to the intrinsic surface properties of solid $Li_2O_2$ or $Li_2S$ such as crystal facets.

**The impact of facets**

We hypothesize that the exposed facets of solid $Li_2O_2$ determine the charge transfer kinetics given the reaction takes place at the surface where certain crystal facets are preferentially exposed. To confirm the impact of facets, we measured the potential-dependent kinetics of $I_3^-$ oxidizing amorphous $Li_2O_2$ that lacks dominant facets and therefore should likely not show thresholds. Amorphous $Li_2O_2$ was synthesized as described earlier and its amorphous state confirmed by XRD, Supplementary Fig. 7[36]. Apparent kinetics $k^{\mathrm{app}}_{\mathrm{I_3^-}-\mathrm{Li_2O_2}}$ is compared with the data from crystalline $Li_2O_2$ in Fig. 2c and shows no sudden acceleration at 3.56 V, confirming the threshold at 3.56 V to be associated with specific abundant facets of crystalline $Li_2O_2$.

To identify the exposed facets, the crystalline $Li_2O_2$ was examined with selected area electron diffraction (SAED) in the transmission electron microscope (TEM). The SAED pattern taken down the $[11\bar{2}0]$ zone axis, Supplementary Fig. 8b, is well indexed to $Li_2O_2$ (P63/mmc). The elongated particle extends in [0001] direction with the $(11\bar{2}0)$ facet dominating the surface followed (0001), Supplementary Fig. 8a. Given that these facets dominate the surface of the $Li_2O_2$ crystallites, their properties should predominantly govern the kinetics.

**Thresholds for $(11\bar{2}0)$ and (0001) facets**

We further explored the chemistry underpinning the threshold potential for $Li_2O_2$ oxidation using density functional theory (DFT) calculations. Particularly, we determined the overpotentials needed to oxidize the dominating facets, in turn rationalizing the threshold potential to activate fast oxidation pathways. We go beyond previous DFT work modelling $Li_2O_2$ oxidation, which only allowed for full removals of the stoichiometric formula via electrochemical steps[37-40]. I.e., two $Li^+$ and one $O_2$ via either $-Li^+$, $-O_2$, $-Li^+$ or $-Li^+$, $-Li^+$, $-O_2$. However, recent experimental work highlighted the dominance of superoxide disproportionation as the $O_2$ evolving step in general and for the formation of the highly reactive singlet oxygen ($^1O_2$) in particular[17,20,31,41,42]. We therefore explicitly allow for disproportionation as well. To do so, we did not limit the charging process to a stoichiometric formula (i.e. two $Li^+$ per $O_2$), but allow for more than two $Li^+$ ions to be removed before $O_2$ evolves.

Using the computational procedure detailed in the Methods, we calculated the reaction energy for each intermediate reaction step. Steps are either electrochemical to desorb Li (one electron and one $Li^+$) or chemical to desorb $O_2$. After each Li removal, the system relaxed to

equilibrium with the remaining atoms reorganizing, releasing the reorganization energy $\Delta E^{j}_{\mathrm{reorg}}$ in the $j^{\mathrm{th}}$ step and the entire slab assuming a new total energy $\Delta E^{j}$. Li is removed from the $Li_2O_2$ surface one after another with the assistance of an overpotential $\eta$. The energy $\Delta E^{j}_{c}$ required to desorb $O_2$ chemically after removing $j$ Li indicates the ease of the overall process to desorb $j$ Li and one $O_2$. At least two Li need to desorb before any O–O moiety could become superoxide-like. Hence, $O_2$ desorbing after two Li would refer to direct oxidation of a peroxide moiety to $O_2$. $O_2$ desorbing after removing four or more Li would refer to disproportionation, leaving behind a Li-deficient $Li_{2-x}O_2$ surface.

We examined the dominant $(11\bar{2}0)$ and (0001) facets whose structures are shown in Fig. 3a,d. The structural unit with the O–O dimer surrounded by six Li atoms is shown in Supplementary Fig. 9. Figures 3b,e give the relaxed energy $\Delta E^{j}$ after the $j^{\mathrm{th}}$ Li removal for four overpotentials up to the minimum overpotential required for up to seven Li removals to become smaller or equal to zero. This number resulted from the number required for the relaxed bond length of one O–O moiety to approach 1.23 Å as found in molecular $O_2$, Fig. 3c. This number also coincides with $\Delta E^{j}_{c}$ becoming lower than 0.2 eV, which is easily overcome thermally, Fig. 3f.

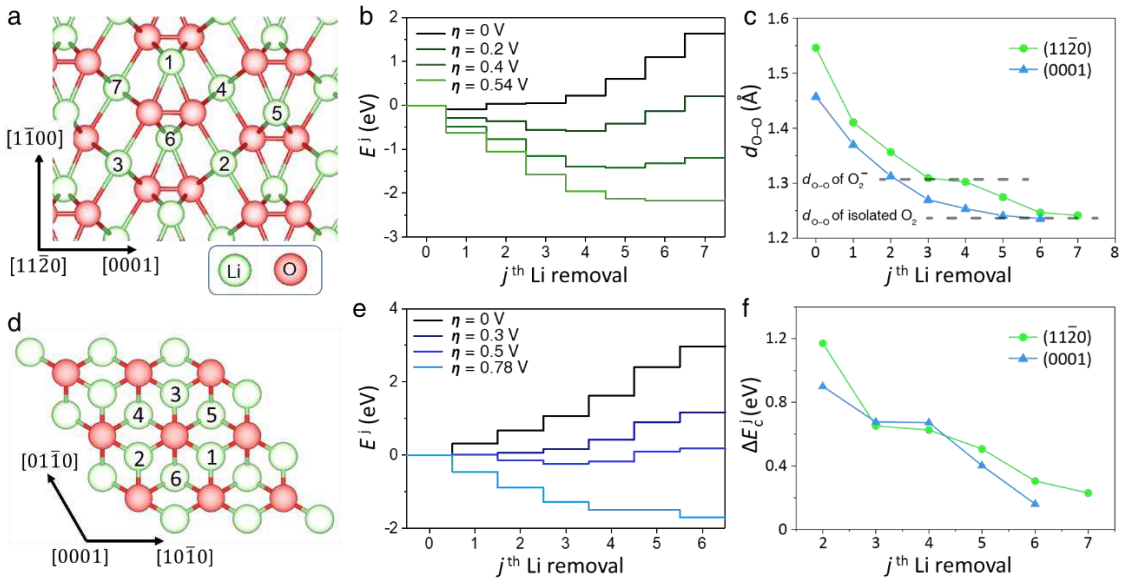


**Fig. 3 | The surface structures and energy profiles during oxidation of specific $Li_2O_2$ facets. a**,**b**, The surface structure of the $(11\bar{2}0)$ facet including the succession of the lowest energy Li extractions (**a**) and the energy profiles during these Li removals under various overpotentials ($\eta$). **d**,**e**, Equivalent surface structure and energy profiles for the (0001) facet. **c**, The evolution of O–O bond lengths of the central O–O moiety in these facets upon Li removal. **f**, The evolution of the chemical energy required to desorb molecular $O_2$ after at least two Li extractions.

We consider first the $(11\bar{2}0)$ facet. With losing three Li, the O–O bond length gradually shortened from 1.54 Å to 1.3 Å (indicating superoxide), Fig. 3c. After four Li removed, formally two adjacent superoxides exist at the surface as also seen in the Bader charge, Supplementary Fig. 10b. Since the $O_2$ desorption energy is with 0.6 eV still significant, spontaneous $O_2$ desorption appears unlikely. However, after removing six to seven Li, the relaxed O–O bond length is close to the 1.23 Å of molecular $O_2$, Fig. 3c, which is no longer strongly chemically bonded, Fig. 3f. Importantly, this

process can be interpreted as disproportionation. As indicated by the Bader charge after removing beyond four Li, one of the two superoxide-like O–O moieties attracts the electron from the nearby one and redistributes the remaining electrons on the surface between the neighbouring O–O moieties. The redistribution is equally seen in the O–O bond lengths; while it decreases continually for the central moiety, the neighbouring ones remain close to the lengths of initial peroxide, Supplementary Fig. 10. This surface disproportionation leaves behind a Li-deficient $Li_2O_2$ surface and an easily released $O_2$ molecule.

Figure 3b shows the corresponding reaction energy profiles for the electrochemical steps at various overpotentials. A minimum overpotential of 0.54 V is required to make the process all the way to seven Li removals energy-downhill, where $O_2$ is released most easily. Lower overpotentials mean higher energy barriers for $O_2$ release, which is associated with low rates. Consequently, the 0.54 V are the overpotential required to activate an overall fast oxidation/$O_2$ release pathway at the $(11\bar{2}0)$ facet. Given this facet to dominate, this overpotential accelerates the decomposition of $Li_2O_2$. This calculation result agrees well with the threshold overpotential of 0.60 V identified in experiments.

Turning to the (0001) facet, Fig. 3c, the O–O moiety is surrounded by six Li atoms. The energy profiles, the O–O bond length, and Bader charge of this process are shown in Fig. 3c,e,f and Supplementary Fig. 10. Since the (0001) facet is Li deficient, the O–O moiety is already closer to a superoxide in terms of initial O–O bond length and Bader charge. According to these measures, the central O–O moiety becomes superoxide-like and isolated $O_2$ after losing two Li and six Li, respectively. Charge redistribution is again seen by the bond length of surrounding O–O moieties remaining close to the initial value, Supplementary Fig. 11. An overpotential of 0.78 V is required to make the energy profile downhill for the entire process to take place spontaneously (Fig. 3d). This predicts a second threshold at 0.78 V (or 3.74 V vs $Li/Li^+$) where $RM^{ox}$ oxidizing $Li_2O_2$ is expected to accelerate further.

To confirm this hypothesis and to identify the second threshold experimentally, TEMPO was used as the RM in TEGDME where we could manipulate $E_{\mathrm{TEMPO/TEMPO^+}}$ to above 3.7 V. Figure 4 shows the measured rate constant over the full voltage range. The first threshold is followed by a gradual increase up to ~3.7 V, where another steep acceleration followed with kinetics doubling. This increase is centred around 3.74 V or an overpotential of 0.78 V and hence matches perfectly the DFT prediction.

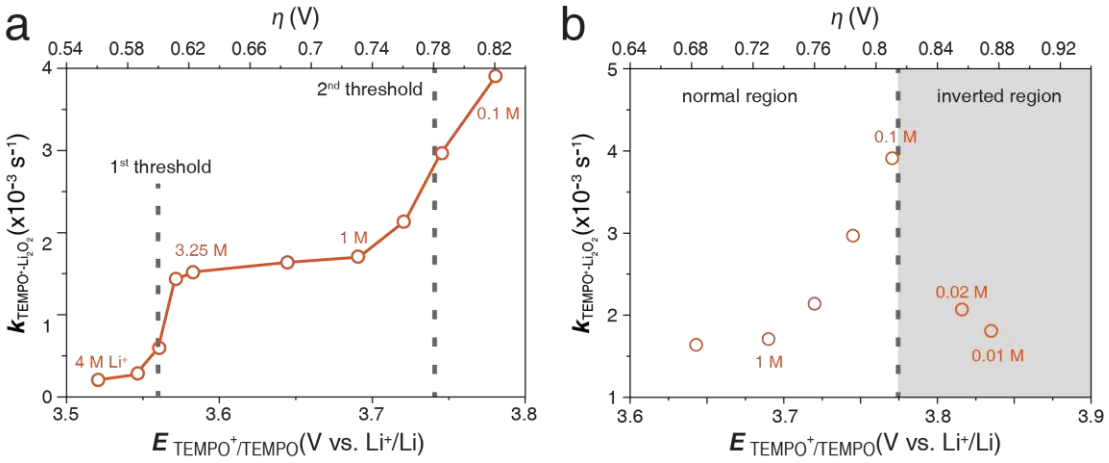


**Fig. 4 | Potential-dependent kinetics of $TEMPO^+$ oxidizing $Li_2O_2$ in tetraglyme over a wide range of $E_{TEMPO/TEMPO^+}$.** **a**,**b**, $TEMPO^+$/TEMPO in tetraglyme electrolytes with various $Li^+$ concentrations from 0.1 M to 4 M (**a**) and 0.01 M to 0.1 M (**b**), where the kinetics decreases after passing a maximum. The dashed lines at 3.56 V and 3.74 V indicate the thresholds of $TEMPO^+$ oxidizing $Li_2O_2$.

Correctly predicting the two thresholds strongly supports the facet-dependent reaction pathways during mediated oxidation of $Li_2O_2$. To better understand the difference between these two facets, it is helpful to consider the reorganization energy $\Delta E^j_{\mathrm{reorg}}$ shown in Supplementary Fig. 10c. For $(0001)$, the reorganization energy is $\approx$–0.4 V throughout, which arises from the symmetric structure of this facet. For $(11\bar{2}0)$ in contrast, reorganization energies are ≈–0.9 V after the 4$^{th}$ and 5$^{th}$ step, where O–O bond length and Bader charger remain nearly constant. The weaker binding of the O–O moieties allows for large spatial reorganization and charge redistribution, which facilitates disproportionation.

Figure 4b not only shows the two thresholds rationalized by the facet-depending oxidation, but also decreasing kinetics beyond ≈3.77 V. Such behaviour is reminiscent of recently shown Marcus inverted region behaviour of peroxide oxidation with different RMs spanning a wide range of redox potentials[20]. Here, we see similar behaviour when the potential of a single RM was tuned using the $Li^+$ concentration. Marcus theory explains such decreasing kinetics despite increasing driving force by the overlap of discrete energy levels in the acceptor and donor[43,44]. A key descriptor herein is the total reorganization energy between initial and product states. Next to the reorganization energy of the $Li_2O_2$ slab as discussed above (Supplementary Fig. 10), it also accounts for the reorganization of the RM and the solvation shell of both reaction partners. Given the complicated multi-step delithiation process until eventual $O_2$ release, rigorous treatment following Marcus theory is beyond the scope of the work, but we suggest that the underlying ideas explain the decreasing kinetics observed here. Overall, the two thresholds and the observed maximum establish target potentials for maximum rates.

## Accelerated kinetics in operation

To test the impact of the potential thresholds on batteries, we charged electrodes preloaded with commercial $Li_2O_2$ using 10 mM TBAI in DMSO containing 1 M or 0.05 M LiTFSI, where the

$I^-/I_3^-$ couple operates below/above the threshold potential. These $Li^+$ concentrations provide in either case sufficient conductivity. If anything, the somewhat lower conductivity of the 0.05 M (higher potential) electrolyte would lessen the effect of accelerated kinetics. Cells were charged using linear sweep voltammetry and $O_2$ evolution followed by DEMS, Fig. 5. Cells without RM served as base case for direct electrooxidization of $Li_2O_2$, Supplementary Fig. 12. Given that above 3.6 V $I_3^-$ is further oxidized to $I_2$, only the $O_2$ evolution below 3.6 V (indicated by the shaded region) is taken to judge kinetics. $I^-$ in 1 M $Li^+$ electrolyte roughly doubled the $O_2$ yield compared to absence of the mediator (Fig. 5b, Supplementary Fig. 12b). Lifting $E_{I^-/I_3^-}$ above the threshold with 0.05 M $Li^+$ raised the $O_2$ yield by as much as 5-fold (Fig. 5a), confirming strongly boosted mediated kinetics above the identified threshold.

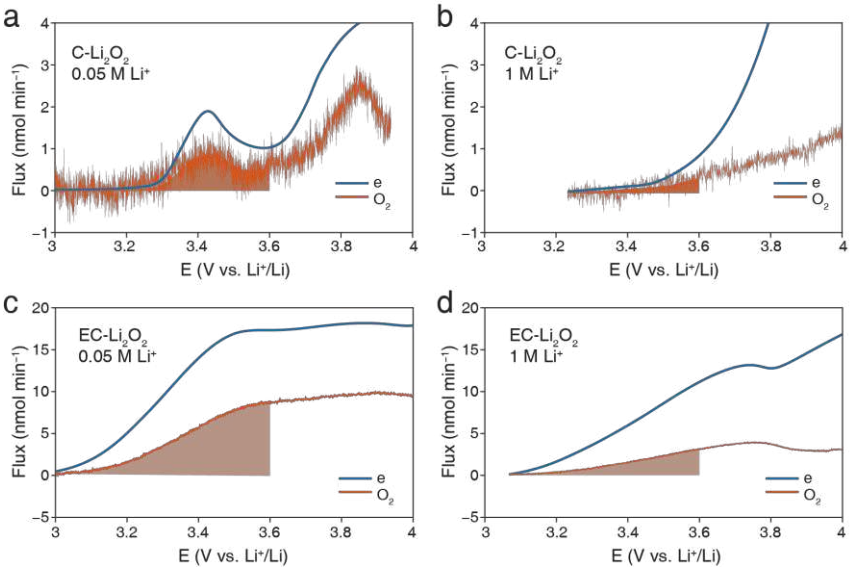


**Fig. 5** | ***In-situ*** **DEMS during mediated charging. a**, **b**, Composite electrodes containing commercial $Li_2O_2$ (C–$Li_2O_2$) and (c)(d) electrochemical-formed $Li_2O_2$ (EC–$Li_2O_2$) were charged in DMSO with 10 mM TBAI and the indicated $Li^+$ concentrations. 0.05 M and 1 M Li+ place $E_{I^-/I_3^-}$ above/below the threshold potential, respectively. The sweep rate was 0.05 mV/s. The shaded regions represent the $O_2$ evolution by the $I_3^-/I^-$ redox couple below 3.6 V.

Electrochemically formed $Li_2O_2$ may expose dominant facets to different extend than chemically formed (commercial) $Li_2O_2$. We therefore did the same experiments except for forming the $Li_2O_2$ by discharging the electrodes in DMSO electrolyte, Fig. 5c,d and Supplementary Fig. 12c,d. At low mediator potential (1 M $Li^+$), the $O_2$ yield doubled against the control without RM while it was boosted more than 5-fold at a high mediator potential (0.05 M $Li^+$). Analogous results in cells using chemically and electrochemically formed $Li_2O_2$ are all in accord with boosted kinetics beyond the threshold that is related with the dominant $(11\bar{2}0)$ facet.

The effect is further confirmed using galvanostatic cycling of cells with the same $I^-$ containing electrolytes, Supplementary Fig. 13. In line with above results, the charging overpotential with lower $Li^+$ concentration (higher $E_{I^-/I_3^-}$) is lower than that with the high $Li^+$ concentration. The charging plateau is with ~3.6 V only slightly above the threshold of 3.56 V. The higher oxidation rate constant allows a smaller overpotential being sufficient to produce a $RM^{ox}$ concentration

capable of oxidizing $Li_2O_2$ at the applied current. This threshold or switch-on effect with $I^-$ only takes $E_{I^-/I_3^-}$ to grow by 10 mV, which we have shown can arise from factors such as $Li^+$ concentration and type of solvents. Therefore, unintentionally positioning $E_{I^-/I_3^-}$ below or above the threshold may explain some contradictory conclusions and debates about the capability of $I_3^-$ oxidizing $Li_2O_2$ during the charging process in literature[35,45], which span from highly active to nearly inactive.

**Conclusions**

In summary, we have shown that the kinetics of mediators oxidizing insulating solids such as $Li_2S$, and $Li_2O_2$ show distinct potential thresholds, where reaction kinetics accelerate several-fold. The step in kinetics happens over a potential change of as little as 10 mV. For mediated $Li_2S$ oxidation, at threshold at 2.99 V (vs $Li^+/Li$) was found, where kinetics accelerated 4.4-fold. For $Li_2O_2$, kinetics increased several-fold at thresholds at 3.56 V and 3.74 V. This phenomenon is independent of the RM and the types of electrolyte. To clarify the origin, we determined the dominant crystal facets of $Li_2O_2$ and examined with DFT the oxidation of the dominant $(11\bar{2}0)$ and (0001) facets. Theoretical overpotentials to activate fast $Li^+/e^-$ extraction followed by $O_2$ release via disproportionation are different at these facets and match the experimentally determined threshold potentials. Disproportionation as the $O_2$ releasing step requires charge redistribution between adjacent, increasingly Li-deficient O–O moieties at the peroxide surface. Facets where these can move more easily such as the $(11\bar{2}0)$ experience larger stabilization by reorganization and tend to be oxidized at lower overpotential.

For mediated oxidation to be fastest, the mediator should exceed the threshold potentials of dominant facets. Adjusting the potential and boosting rate capability may be as simple as reducing the $Li^+$ concertation as long as ionic conductivity remains sufficient. The results resolve contradictory conclusions in the literature about the ability of the $I_3^-/I^-$ redox couple to oxidize $Li_2O_2$. We give a rational for the most effective use of RMs to oxidize insulating active materials such as those in metal-sulfur, metal-air, or metal-$CO_2$ batteries. The properties and abundance of individual facets of the solid product determine required RM potentials for maximum charging rates.

**Methods**

**Materials and syntheses.** Chemicals were from Sigma Aldrich and used without further purification. Lithium Superionic Conductor (LiSICON) was from Ohara. Gas diffusion layer (GDL) electrodes (Freudenberg, H2315) were from Quintech. DMSO was distilled under vacuum and DME was distilled under argon. All the solvents were further dried for several days with activated type 4Å molecular sieves in an Ar-filled glove box. The molecular sieves (Aladdin) were first washed with ethanol, dried in the furnace at 550 °C for 5 hours, and then placed in a drying tube and further dried at 300 °C with a Büchi oven under vacuum for 24 h and transferred into an Ar-filled glovebox without exposure to air. The final water content of the DMSO and DME after drying was < 4 ppm (determined using a Mettler Toledo Karl Fischer titrator). Bistrifluoromethanesulfonimide lithium (LiTFSI) was dried under

vacuum for 24 h at 120 °C. $TEMPO^+$ was prepared by electrolysis in a glass H-cell with a carbon paper working electrode, a commercial AgCl/Ag-acetonitrile reference electrode, and a graphite rod counter electrode. The working and counter electrode were separated with a sintered glass frit. 20 mM TEMPO in 0.1 M LiTFSI/tetraglyme served as anolyte at the working electrode and 0.1 M LiTFSI-tetraglyme served as catholyte at the counter electrode. Both electrolytes were stirrd. Firstly, the redox potential of $TEMPO^+$/TEMPO was determined by using cyclic voltammetry (CV) using an electrochemical workstation (VMP3, Biologic, France) with a planar glassy carbon disc electrode (diameter 3mm). Then the carbon paper working electrode was held at 400 mV positive to the redox potential of TEMPO to obtain $TEMPO^+$. Finally, the concentration of $TEMPO^+$ was determined using CV and found to be around 8 mM.

Amorphous $Li_2O_2$ was synthesized via a rapid disproportionation reaction of tetramethyl-ammonium superoxide ($TMAO_2$) and $LiClO_4$ in acetonitrile in an Ar-filled glove box as described previously[1]. $TMAO_2$ was prepared according to the solid reaction: $[(Me_4N)OH]\cdot H_2O + 3\ KO_2 \rightarrow (Me_4N)O_2 + 3/2\ O_2 + 3\ KOH$. Briefly, 10.9 g $[(Me_4N)OH]\cdot H_2O$ and 35 g $KO_2$ (5-fold excess $(Me_4N)OH]\cdot H_2O$) were ground separately in mortars to fine powders in an Ar-filled glove box and then transferred to a 500 mL round-bottom flask with 20 g of 3 mm-diameter glass beads. The mixture was stirred with an overhead stirrer in the glovebox for a week. Finally, the mixture was transferred into a Soxhlet extractor and $TMAO_2$ was extracted using liquid ammonia. 2.3 g $TMAO_2$ was obtained and sealed under vacuum prior to transfer to the glovebox.

**Characterizations.** For the surface characterizations, the $Li_2O_2$ disk was immersed in DMSO for 10 minutes for TOF-SIMS experiments. Both a pristine disk and a treated disk were characterized with TOF-SIMS 5-100 (ION-TOF GmbH). X-ray diffraction (XRD) was carried out in an air-tight holder with a low-background Si substrate at a Bruker D4 X-ray diffractometer (Bruker, Germany) with Ni-filtered Cu $K_\alpha$ radiation (40 kV, 40 mA). The morphology of commercial $Li_2O_2$ was characterized by TEM (JEOL JEM 2100).

The kinetics of $DFc^+$ oxidizing $Li_2S$ is measured by using UV-vis spectroscopy. The $DFc^+$ solution was prepared by electrolysis of 10 mM DFc in 0.1 M LiTFSI/DME in a homemade H-type cell with a piece of LiSICON solid state electrolyte to separate the catholyte and anolyte and a carbon paper working electrode and a Li counter electrode. The final concentration of $DFc^+$ was determined using CV. 3mL of solution containing a known concentration of $DFc^+$ was injected to an air–tight cuvette containing 10 mg of $Li_2S$ under stirring in an Ar-filled glovebox. After reaction with several minutes, the suspension is centrifuged briefly and the UV-vis spectra of the clear solution was recorded. The remaining concentrations of $DFc^+$ after reaction were determined form the absorption peak at 780 nm and $-\ln A_{780nm}$ was plotted versus the reaction time, Supplementary Fig. 2. The rate constant ($k^{\mathrm{app}}_{\mathrm{DFc-Li_2S}}$) was obtained from the slope of the data fit as 1st order reaction. The polysulfide solution was prepared by stirring the $S_8$ powder and $Li_2S$ together in DME overnight. $Li_2S$ reacted with $S_8$ to form polysulfides.

The suspension was centrifuged and then the brownish supernatant was collected. The $DFc^+$ solution was injected into the polysulfide solution and then colour of $DFc^+$ faded out rapidly within 150 s, Supplementary Fig. 3.

**Electrochemical methods.** The differential electrochemical mass spectrometry (DEMS) system was based on a commercial magnet-sector mass spectrometer (Thermo Fischer, Prima BT) and guided by the requirement to quantify all the gases evolved during the charging process. The DEMS cell was based on a customized Swagelok-type cell providing air-tightness, as discussed previously[2]. In the DEMS experiments of $I_3^-$ oxidizing $Li_2O_2$, 0.8 ml of various solutions containing 4 mM $TBAI_3$ were injected into a vial containing an excess amount of $Li_2O_2$. The evolved $O_2$ was quantified using DEMS. Pure Ar was used as a carrier gas and the flow rate was typically 1 mL/min. Kinetics measurements are discussed in Supplementary Note 1. Typically, 9 mg of $Li_2O_2$ was used. In the experiment of $TBAI_3$ oxidizing LiOH, $Li_2CO_3$, Li formate, and Li acetate, the same experiments were carried out with $Li_2O_2$ being replaced by these compounds. In the experiments of $TEMPO^+$ oxidizing $Li_2O_2$, 0.8 ml of 8 mM $TEMPO^+$ in tetraglyme with various $Li^+$ concentrations between 3.25 M and 4 M $Li^+$ were injected into a vial containing 9 mg $Li_2O_2$ and the $O_2$ evolution was quantified.

*In-situ* DEMS experiments were carried out with electrodes preloaded with commercial $Li_2O_2$ or electrochemically formed $Li_2O_2$ (EC-$Li_2O_2$). To load commercial $Li_2O_2$, 10 mg $Li_2O_2$ were dispersed in 5 ml of DME by stirring and ultra-sonication. Then 50 µl of the suspension were dropped onto a GDL electrode (12 mm diam.). The wet electrode is dried under vacuum and the same procedure repeated several times. The mass loading of $Li_2O_2$ was 1 mg $cm^{-2}$. To load EC-$Li_2O_2$, the electrode was discharged in 1 M LiTFSI tetraglyme electrolyte saturated with $O_2$ to a capacity of 1.16 mAh $cm^{-2}$ (corresponding to 1 $mg_{Li2O2}$ $cm^{-2}$). The electrodes with $Li_2O_2$ were charegd using a linear voltage sweep from OCV to 4 V (vs. $Li^+/Li$) at a sweep rate of 0.05 mV/s. Pure Ar worked as carrier gas at a flow rate of 0.3 ml/min.

Scanning Electrochemical Microscope (SECM) approach curves towards a $Li_2O_2$ pellet were measured with a CHI 900D SECM in an Ar-filled glovebox as described previously[3]. $Li_2O_2$ disks were obtained by pressing $Li_2O_2$ powder with a die set press in an Ar-filled glove box. Disks of 13 mm diameter and ~1 mm thickness were prepared and served as substrate. An Au microelectrode (diam. 25 µm, CHI) served as the SECM probe. Prior to the measurements, the Au tip was polished with a homemade microelectrode beveller and checked with a microscope. A silver wire reference electrode (RE) and a platinum counter electrode (CE) were used. The data processing and fitting process were described elsewhere[4]. A dimensionless rate constant, κ, was obtained by data fit, which equals to $\frac{k^{\mathrm{app}}\, r_0}{D}$, where $r_0$ is the radius of tip, $D$ is the diffusion coefficient of redox mediator, and $k^{\mathrm{app}}$ the apparent heterogeneous rate constant.

$E_{\mathrm{DFc/DFc^+}}$ and $E_{\mathrm{TEMPO/TEMPO^+}}$ (vs $Li^+/Li$) in various electrolytes were measured by CV using a three-electrode configuration using a glassy carbon working electrode and a graphite rod counter electrode. The piece of partially delithiated $Li_{1-x}FePO_4$ composite electrode inside a glass tube with a frit

at the end was used as the reference electrode, which provided a constant potential of 3.45 V vs $Li^+/Li$. The reference electrode was filled with the same electrolyte as the working electrode but without a redox mediator. Because the $I_3^-/I^-$ redox couple does not show a pair of symmetric redox peaks, $E_{I^-/I_3^-}$ in various solvents was calculated from the open-circuit voltage (OCV). A solution containing 10 mM $TBAI_3$ and 10 mM TBAI was prepared with various concentrations of LiTFSI. The OCV was recorded and the $E_{I^-/I_3^-}$ (*vs* $Li^+/Li$) can be calculated from $E_{OCV}$ by the Nernst equation:

$$E_{OCV} = E_{I_3^-/I^-} + \frac{RT}{2F}\ln\frac{C_{TBAI_3}}{(C_{TBAI})^3} \quad \text{(S1)}$$

Cycling performance was measured with homemade Swagelok-type cells assembled in an Ar-filled glove box. Super P-PTFE (9:1, wt%) was sprayed with a mass loading of 0.5 mg/cm$^2$ on GDL as cathode. The anode was Li metal. The electrodes were separated by a LiSICON glass to prevent the shuttling and short-circuit of RMs. The *iR* drop caused by LiSICON was corrected in the load curves. 10 mM TBAI-DMSO with 0.05 M or 1 M LiTFSI was used as catholyte and 0.5 M LiTFSI-DME as anolyte. The cells were cycled at a current density of 0.2 mA/cm$^2$ in 1 atm of $O_2$.

**Density Functional Theory (DFT) calculations.** DFT calculations were conducted within the Vienna Ab-initio Simulation Package (VASP)[5,6] The potentials were of the projector plane wave (PAW) type,[7] and the exchange-correlation part of the density functional was treated within the generalized gradient approximation (GGA) of Perdew–Burke–Ernzerhof (PBE).[8] We used plane-wave cutoff energy of 500 eV and 1×1×1 Monkhorst–Pack k-point mesh[9] with Gaussian smearing of 0.05 eV [10] to relax the electronic energies and nuclear degrees of freedom. The electronic structure was optimized within an error of $10^{-6}$ eV/atom and the geometry was optimized to force tolerance of 0.03 eV/Å. The spin-polarization was considered and DFT-D3 method[11] with Becke-Jonson damping[12] was applied to describe the van der Walls (vdW) interactions. Procedures of all the calculations were implemented in the computational platform for battery materials.[13]

For examining the decomposition mechanisms of $Li_2O_2$ on the $(11\bar{2}0)$ facet, a slab supercell (2×2) with 5 layers containing 160 atoms was constructed from a hexagonal unit cell (a = 3.12 Å, c = 7.56 Å) and the vacuum slab was set to 20 Å to eliminate the ramped electron interaction between slabs due to the periodic system. Two layers were fixed to mimic the bulk structure. The path starts with $Li^+$ removal from the surface structure and ends with $O_2$ evolution, covering both the electrochemical (the desorption of $Li^+$) and the chemical (the desorption of $O_2$) steps. As long as the process is energy favorable, the O-O dimer could be removed at any stage and the energy required is shown in Supplementary Fig. 10. The details will be discussed below.

First, we calculated the redox potential of the bulk $Li_2O_2$ decomposition according to the reaction

$$Li_2O_2 \longrightarrow 2Li + O_2\uparrow \quad \text{(S2)}$$

The reaction free energy of the above reaction is

$$\Delta G = G(\mathrm{Li}) + G(\mathrm{O_2}) - G(\mathrm{Li_2O_2}) \quad \text{(S3)}$$

where the Gibbs free energies of Li and $Li_2O_2$ are calculated according to

$$G = E + ZPE + \Delta H_{\mathrm{expt}}^{0\to 298.15K} - TS_{\mathrm{expt}}^{0\to 298.15K} \quad \text{(S4)}$$

where the *E* is the electronic energy obtained from the DFT calculations, ZPE is the zero-point energy, $\Delta H_{\mathrm{expt}}^{0\to 298.15K}$ and $S_{\mathrm{expt}}^{0\to 298.15K}$ are the experimental enthalpy and entropy variation from 0 K to 298.15 K, respectively.[14] *T* is 298.15 K.

$O_2$ (1 atm, 298.15 K) was corrected by the following reaction due to the overestimate of the binding energy by DFT:

$$Li_2O + ½\ O_2 \longrightarrow Li_2O_2 \quad \text{(S5)}$$

Based on the experimental reaction energy of the above reaction ($\Delta G_r^{\mathrm{expt}}$) and the calculated Gibbs free energies of $Li_2O$ and $Li_2O_2$, which are involved in the correction of the zero-point energy and the experimental enthalpy and entropy,[46] we determine the chemical potential of oxygen according to

$$\mu(\mathrm{O}) = G(\mathrm{Li_2O_2}) - G(\mathrm{Li_2O}) - \Delta G_r^{\mathrm{expt}} \quad \text{(S6)}$$

Thus, the Gibbs free energy of $O_2$ is

$$G(\mathrm{O_2}) = 2\ \mu(\mathrm{O}) + ZPE + \Delta H_{\mathrm{expt}}^{0\to 298.15K} - TS_{\mathrm{expt}}^{0\to 298.15K} \quad \text{(S7)}$$

where the enthalpy and entropy are referred to as the thermochemical dataset.[46] *T* is 298.15K. Then the theoretical redox potential (*U*) can be calculated by:

$$U = -\Delta G/nF \quad \text{(S8)}$$

Following the above equations (S2)-(S8), we give the theoretical redox potential of 2.75 V for the bulk $Li_2O_2$ decomposition, close to the reported value in the literature (2.82 V)[15].

After obtaining the bulk redox potential, the next step is to explore the intrinsic barrier of the surface decomposition. It is widely accepted that the $Li_2O_2$ decomposition includes both the electrochemical step (the desorption of $Li^+$) and the chemical step (the desorption of $O_2$), respectively. The reaction energy of the $j^{th}$ (*j* ranges from 1 to 7) electrochemical step ($\Delta E_e^j$) is defined as

$$\Delta E_e^j = E^j + E(\mathrm{Li}) - E^{j-1} - eU \quad \text{(S9)}$$

where $E^j$ and $E^{j-1}$ are the energies of the $Li_2O_2$ slab after and before the desorption of Li, respectively, $E(\mathrm{Li})$ is the energy of bulk Li, and *U* is the predicted theoretical electrochemical potential. The chemical step for the $j^{\mathrm{th}}$ step is defined as:

$$\Delta E_c^j = E_C^{j(j+2)} + E(\mathrm{O_2}) - E_C^{j(j+1)} \quad \text{(S10)}$$

where $E_C^{j(j+2)}$ and $E_C^{j(j+1)}$ are the energies of the $Li_2O_2$ slab after and before the desorption of $O_2$, respectively. To cancel systematic errors, the reference $E(\mathrm{O_2})$ is the energy of the directly calculated energy of $O_2$ in the gas phase without correction. Note that the $O_2$ which is about to desorb is in an

isolated state and physically adsorbed at the surface as confirmed by the differential charge density (Supplementary Fig. 10). It can be seen that there is almost no charge density between the $O_2$ and the matrix, suggesting that the $O_2$ in the surface described by DFT is similar to the directly calculated state in DFT within a supercell, which we chose a sufficiently large cubic cell (20×20×20 $Å^3$) to mimick the process taking place at an extended surface.

Correspondingly, the overpotential ($\eta$) is defined as

$$\eta = \max\{\Delta E_e^j/e\} \quad \text{(S11)}$$

It is worth mentioning that the conventional reaction profiles are confined to a single or two $Li_2O_2$ formula(s)[15-17], thus including only three steps (Li↑-$O_2$↑-Li↑ or Li↑-Li↑-$O_2$↑, where the up-arrow denotes the desorption) or a repeat of these three steps to maintain the ratio of desorbed Li atoms to $O_2$ molecules at 2:1. In such a path, the reaction energy of the chemical step is up to 1.8 eV,[39] which is impossible to overcome by the energy oscillation, implying a non-spontaneous process. In other words, the conventional reaction profiles are non-spontaneous.

Herein, based on the consideration that the exploration of the path should not be limited to the stoichiometric formulas, *i.e.*, the ratio of desorbed Li atoms to $O_2$ molecules can exceed 2:1, we demonstrate that the rate-determining step (rds) is the electrochemical desorption of Li rather than the chemical desorption of $O_2$. Figure 3 shows an irregular but more feasible path followed during the decomposition process at the conversion reaction cathode, where the decomposition occurs from the electrochemical step until the surface becomes amorphous and the chemical step is no longer the rds. Figure 3f shows the dependence of the chemical reaction energy ($\Delta E_c^j$) for the desorption of $O_2$ after removal of *j* Li. It is seen that $\Delta E_c^j$ drops from 1.82 to 0.20 eV as the number of the electrochemical Li extractions increased from 2 to 7. This barrier of 0.2 eV is sufficiently small to be easily overcome by thermal oscillations. Also, compared with the electrochemical step (0.63 eV), the chemical step (0.20 eV) is no longer the rds. These results in turn demonstrate that the required driving force during charging is dictated by the electrochemical potential barrier.

## References


1 Choi, J. W. & Aurbach, D. Promise and reality of post-lithium-ion batteries with high energy densities. *Nat. Rev. Mater.* **1**, 16013, doi:10.1038/natrevmats.2016.13 (2016).

2 Qiao, Y., Jiang, K., Deng, H. & Zhou, H. A high-energy-density and long-life lithium-ion battery via reversible oxide–peroxide conversion. *Nature Catalysis* **2**, 1035-1044, doi:10.1038/s41929-019-0362-z (2019).

3 Cameron, J. M. *et al.* Molecular redox species for next-generation batteries. *Chem. Soc. Rev.*, doi:10.1039/D0CS01507E (2021).

4 Kwak, W.-J. *et al.* Lithium–Oxygen Batteries and Related Systems: Potential, Status, and Future. *Chem. Rev.*, doi:10.1021/acs.chemrev.9b00609 (2020).

5 Ko, Y. *et al.* Anchored Mediator Enabling Shuttle-Free Redox Mediation in Lithium-Oxygen Batteries. *Angew. Chem. Int. Ed.* **59**, 5376-5380, doi:10.1002/anie.201916682 (2020).
6 Wang, Y. & Lu, Y.-C. Nonaqueous Lithium–Oxygen batteries: Reaction mechanism and critical open questions. *Energy Storage Materials* **28**, 235-246, doi:10.1016/j.ensm.2020.03.007 (2020).
7 Wu, S. *et al.* Organic hydrogen peroxide-driven low charge potentials for high-performance lithium-oxygen batteries with carbon cathodes. *Nat. Commun.* **8**, 15607, doi:10.1038/ncomms15607 (2017).
8 Qiao, Y. *et al.* Li-$CO_2$ Electrochemistry: A New Strategy for $CO_2$ Fixation and Energy Storage. *Joule*, doi:10.1016/j.joule.2017.07.001 (2017).
9 Lu, Y.-C., He, Q. & Gasteiger, H. A. Probing the Lithium–Sulfur Redox Reactions: A Rotating-Ring Disk Electrode Study. *J. Phys. Chem. C* **118**, 5733-5741, doi:10.1021/jp500382s (2014).
10 Bonnick, P. & Muldoon, J. The Dr Jekyll and Mr Hyde of lithium sulfur batteries. *Energy Environ. Sci.* **13**, 4808-4833, doi:10.1039/D0EE02797A (2020).
11 Kwak, W.-J. *et al.* Controllable and stable organometallic redox mediators for lithium oxygen batteries. *Materials Horizons* **7**, 214-222, doi:10.1039/C9MH01043B (2020).
12 Park, J.-B., Lee, S. H., Jung, H.-G., Aurbach, D. & Sun, Y.-K. Redox Mediators for Li–$O_2$ Batteries: Status and Perspectives. *Adv. Mat.* **30**, 1704162, doi:10.1002/adma.201704162 (2018).
13 Kwak, W.-J., Kim, H., Jung, H.-G., Aurbach, D. & Sun, Y.-K. Review—A Comparative Evaluation of Redox Mediators for Li-$O_2$ Batteries: A Critical Review. *J. Electrochem. Soc.* **165**, A2274-A2293, doi:10.1149/2.0901810jes (2018).
14 Meini, S., Elazari, R., Rosenman, A., Garsuch, A. & Aurbach, D. The Use of Redox Mediators for Enhancing Utilization of $Li_2S$ Cathodes for Advanced Li–S Battery Systems. *J. Phys. Chem. Lett.* **5**, 915-918, doi:10.1021/jz500222f (2014).
15 Pande, V. & Viswanathan, V. Criteria and Considerations for the Selection of Redox Mediators in Nonaqueous Li–$O_2$ Batteries. *ACS Energy Lett.* **2**, 60-63, doi:10.1021/acsenergylett.6b00619 (2017).
16 McCloskey, B. D. *et al.* Twin Problems of Interfacial Carbonate Formation in Nonaqueous Li–$O_2$ Batteries. *J. Phys. Chem. Lett.* **3**, 997-1001, doi:10.1021/jz300243r (2012).
17 Wang, Y., Lu, Y.-R., Dong, C.-L. & Lu, Y.-C. Critical Factors Controlling Superoxide Reactions in Lithium–Oxygen Batteries. *ACS Energy Lett.*, 1355-1363, doi:10.1021/acsenergylett.0c00365 (2020).
18 Liang, Z., Zhou, Y. & Lu, Y.-C. Dynamic oxygen shield eliminates cathode degradation in lithium–oxygen batteries. *Energy Environ. Sci.* **11**, 3500-3510, doi:10.1039/C8EE02067A (2018).
19 Gao, X., Chen, Y., Johnson, L. R., Jovanov, Z. P. & Bruce, P. G. A rechargeable lithium–oxygen battery with dual mediators stabilizing the carbon cathode. *Nat. Energy* **2**, 17118, doi:10.1038/nenergy.2017.118 (2017).
20 Petit, Y. K. *et al.* Mechanism of mediated alkali peroxide oxidation and triplet versus singlet oxygen formation. *Nat. Chem.* **13**, 465–471, doi:10.1038/s41557-021-00643-z (2021).
21 Liang, Z. & Lu, Y.-C. Critical Role of Redox Mediator in Suppressing Charging Instabilities of Lithium–Oxygen Batteries. *J. Am. Chem. Soc.* **138**, 7574-7583, doi:10.1021/jacs.6b01821 (2016).
22 Kwak, W.-J. *et al.* Deactivation of redox mediators in lithium-oxygen batteries by singlet oxygen. *Nat. Commun.* **10**, 1380, doi:10.1038/s41467-019-09399-0 (2019).
23 Liang, Z., Zou, Q., Xie, J. & Lu, Y.-C. Suppressing singlet oxygen generation in lithium–oxygen

batteries with redox mediators. *Energy Environ. Sci.* **13**, 2870-2877, doi:10.1039/D0EE01114B (2020).

24 Mu, X., Pan, H., He, P. & Zhou, H. Li–$CO_2$ and Na–$CO_2$ Batteries: Toward Greener and Sustainable Electrical Energy Storage. *Adv. Mat.* **32**, 1903790, doi:https://doi.org/10.1002/adma.201903790 (2020).

25 Zhao, M., Chen, X., Li, X. Y., Li, B. Q. & Huang, J. Q. An Organodiselenide Comediator to Facilitate Sulfur Redox Kinetics in Lithium-Sulfur Batteries. *Adv. Mat.* **33**, doi:10.1002/adma.202007298 (2021).

26 Zhao, M. *et al.* Redox Comediation with Organopolysulfides in Working Lithium-Sulfur Batteries. *Chem* **6**, 3297-3311, doi:10.1016/j.chempr.2020.09.015 (2020).

27 Tsao, Y. *et al.* Designing a Quinone-Based Redox Mediator to Facilitate $Li_2S$ Oxidation in Li-S Batteries. *Joule*, doi:10.1016/j.joule.2018.12.018.

28 Chen, Y., Gao, X., Johnson, L. R. & Bruce, P. G. Kinetics of lithium peroxide oxidation by redox mediators and consequences for the lithium–oxygen cell. *Nat. Commun.* **9**, 767, doi:10.1038/s41467-018-03204-0 (2018).

29 Henstridge, M. C., Laborda, E., Rees, N. V. & Compton, R. G. Marcus–Hush–Chidsey theory of electron transfer applied to voltammetry: A review. *Electrochim. Acta* **84**, 12-20, doi:10.1016/j.electacta.2011.10.026 (2012).

30 Wild, M. *et al.* Lithium sulfur batteries, a mechanistic review. *Energy Environ. Sci.* **8**, 3477-3494, doi:10.1039/C5EE01388G (2015).

31 Wang, Y. *et al.* A Solvent-Controlled Oxidation Mechanism of $Li_2O_2$ in Lithium–Oxygen Batteries. *Joule* **2**, 2364-2380, doi:10.1016/j.joule.2018.07.021 (2018).

32 Zou, Q. & Lu, Y.-C. Solvent-Dictated Lithium Sulfur Redox Reactions: An Operando UV–vis Spectroscopic Study. *J. Phys. Chem. Lett.* **7**, 1518-1525, doi:10.1021/acs.jpclett.6b00228 (2016).

33 Ko, Y. *et al.* A comparative kinetic study of redox mediators for high-power lithium–oxygen batteries. *J. Mat. Chem. A* **7**, 6491-6498, doi:10.1039/C9TA00096H (2019).

34 Bawol, P. P. *et al.* A new thin layer cell for battery related DEMS-experiments: the activity of redox mediators in the Li–$O_2$ cell. *Phys. Chem. Chem. Phys.* **20**, 21447-21456, doi:10.1039/C8CP03592J (2018).

35 Leverick, G., Tułodziecki, M., Tatara, R., Bardé, F. & Shao-Horn, Y. Solvent-Dependent Oxidizing Power of LiI Redox Couples for Li–$O_2$ Batteries. *Joule* **3**, 1106-1126, doi:10.1016/j.joule.2018.12.014 (2019).

36 Zhang, Y. *et al.* Amorphous $Li_2O_2$: Chemical Synthesis and Electrochemical Properties. *Angew. Chem. Int. Ed.* **55**, 10717-10721, doi:10.1002/anie.201605228 (2016).

37 Kang, S., Mo, Y., Ong, S. P. & Ceder, G. A Facile Mechanism for Recharging $Li_2O_2$ in Li–$O_2$ Batteries. *Chem. Mat.* **25**, 3328–3336, doi:10.1021/cm401720n (2013).

38 Hummelshoj, J. S., Luntz, A. C. & Norskov, J. K. Theoretical evidence for low kinetic overpotentials in Li-$O_2$ electrochemistry. *J. Chem. Phys.* **138**, 034703 (2013).

39 Zhu, J., Ren, X., Liu, J., Zhang, W. & Wen, Z. Unraveling the Catalytic Mechanism of Co3O4 for the Oxygen Evolution Reaction in a Li–O2 Battery. *ACS Catal.* **5**, 73-81, doi:10.1021/cs5014442 (2015).

40 Zhu, J. *et al.* Surface Acidity as Descriptor of Catalytic Activity for Oxygen Evolution Reaction in Li-O2 Battery. *J. Am. Chem. Soc.* **137**, 13572-13579, doi:10.1021/jacs.5b07792 (2015).

41 Mourad, E. *et al.* Singlet oxygen from cation driven superoxide disproportionation and

consequences for aprotic metal–$O_2$ batteries. *Energy Environ. Sci.* **12**, 2559-2568, doi:10.1039/C9EE01453E (2019).

42 Mahne, N. *et al.* Singlet oxygen generation as a major cause for parasitic reactions during cycling of aprotic lithium–oxygen batteries. *Nat. Energy* **2**, 17036, doi:10.1038/nenergy.2017.36 (2017).

43 Marcus, R. A. Electron transfer reactions in chemistry. Theory and experiment. *Rev. Mod. Phys.* **65**, 599-610, doi:10.1103/RevModPhys.65.599 (1993).

44 Savéant, J.-M. & Constentin, C. *Elements of molecular and biomolecular electrochemistry*. 2nd edn, (John Wiley & Sons, 2019).

45 Burke, C. M. *et al.* Implications of 4 $e^-$ Oxygen Reduction via Iodide Redox Mediation in Li–$O_2$ Batteries. *ACS Energy Lett.* **1**, 747-756 (2016).

46 Chase, M. W. (American Institute of Physics: Melville, NY, 1998).

## Acknowledgments

This work was financially supported by the National Natural Science Foundation of China (51773092, 21975124, 11874254, 51802187, U2030206). S.A.F. is indebted to IST Austria for support.

## Author contributions

Y.C., S.S. and S.A.F. conceived and directed the project. D.C., X.S., A.W. and F.Y. performed experiments and DFT calculations. S.A.F, Y.C., and S.S wrote the manuscript. All authors discussed and revised the manuscript.

## Competing interests

The authors declare no competing interests.

# Supplementary Files

This is a list of supplementary files associated with this preprint. Click to download.

- SupplementaryInformation.pdf